A PLETHORA-Auxin Transcription Module Controls Cell Division Plane Rotation through MAP65 and CLASP

Pankaj Dhonukshe,[1,*] Daan A. Weits,[1] Alfredo Cruz-Ramirez,[1] Eva E. Deinum,[2] Simon Tindemans,[2,6] Klementina Kakar,[1] Kalika Prasad,[1,7] Ari Pekka Mähönen,[1,8] Chris Ambrose,[3] Michiko Sasabe,[4] Guy Wachsmann,[1] Marijn Luijten,[1] Tom Bennett,[1,9] Yasunori Machida,[4] Renze Heidstra,[1] Geoffrey Wasteneys,[3] Bela M. Mulder,[2,5] and Ben Scheres[1,*]

[1]Department of Biology, Utrecht University, Padualaan 8, 3584 CH Utrecht, The Netherlands
[2]FOM Institute AMOLF, Science Park 104, 1098 XG Amsterdam, The Netherlands
[3]Department of Botany, University of British Columbia, 6270 University Boulevard, Vancouver, British Columbia V6T 1Z4, Canada
[4]Division of Biological Science, Graduate School of Science, Nagoya University, Nagoya, 464-8602, Japan
[5]Laboratory of Plant Cell Biology, Wageningen University, Droevendaalsesteeg 1, 6708 PB Wageningen, The Netherlands
[6]Present address: Department of Electrical and Electronic Engineering, Imperial College, South Kensington Campus, London SW7 2AZ, UK
[7]Present address: School of Biology, Indian Institute of Science Education and Research, Thiruvananthapuram 695016, Kerala, India
[8]Present address: Institute of Biotechnology, University of Helsinki, Helsinki FIN-00014, Finland
[9]Present Address: Department of Plant Sciences, University of Cambridge, Downing Site, Downing Street, Cambridge CB2 3EA, UK
*Correspondence: p.b.dhonukshe@uu.nl (P.D.), b.scheres@uu.nl (B.S.)
DOI 10.1016/j.cell.2012.02.051

SUMMARY

Despite their pivotal role in plant development, control mechanisms for oriented cell divisions have remained elusive. Here, we describe how a precisely regulated cell division orientation switch in an *Arabidopsis* stem cell is controlled by upstream patterning factors. We show that the stem cell regulatory PLETHORA transcription factors induce division plane reorientation by local activation of auxin signaling, culminating in enhanced expression of the microtubule-associated MAP65 proteins. MAP65 upregulation is sufficient to reorient the cortical microtubule array through a CLASP microtubule-cell cortex interaction-dependent mechanism. CLASP differentially localizes to cell faces in a microtubule- and MAP65-dependent manner. Computational simulations clarify how precise 90° switches in cell division planes can follow self-organizing properties of the microtubule array in combination with biases in CLASP localization. Our work demonstrates how transcription factor-mediated processes regulate the cellular machinery to control orientation of formative cell divisions in plants.

INTRODUCTION

The orientation of cell division plane is key to the generation of multicellular organisms as their randomization often leads to morphogenetic defects (Baena-López et al., 2005; Torres-Ruiz and Jürgens, 1994; Traas et al., 1995). In plants, neighboring cells cannot relocate due to shared cell walls, and cell divisions have to be oriented parallel to the surface ("periclinal") to create new layers. Asymmetric periclinal cell divisions, where daughter cells acquire distinct identities, have been termed "formative divisions" (Gunning et al., 1978). Most formative divisions occur at early embryo stages when the body plan is established (Jürgens, 1995), but others take place when lateral organs are generated (De Smet and Beeckman, 2011). New layers are repeatedly established in the ground tissue and epidermis/lateral root cap (LRC) stem cells of *Arabidopsis* roots (Dolan et al., 1993). Several transcription factors required for these divisions have been identified (Di Laurenzio et al., 1996; Helariutta et al., 2000; Willemsen et al., 2008) but mechanisms by which the orientation of cell division planes are controlled have remained unknown.

Plant cell division planes are specified prior to mitosis by formation of a cortical microtubular band called preprophase band (PPB) (Pickett-Heaps and Northcote, 1966). The cortical division site remains marked throughout mitosis and cytokinesis after the PPB has disassembled (Smith, 2001), with negative and positive markers of the cortical division site memorizing PPB position to guide the cell plate (Müller et al., 2009). Most of those proteins follow the localization of PPB microtubules and seem to operate downstream (Rasmussen et al., 2011a; Rasmussen et al., 2011b). These observations indicate how the microtubular PPB can be coupled with cytokinesis but do not reveal how the PPB is oriented.

Cell divisions associated with the *Arabidopsis* root stem cell niche are sustained by the activity of PLETHORA (PLT) proteins, members of the AP2 transcription factor family (Aida et al., 2004; Galinha et al., 2007). Initial induction of *PLT* expression is regulated by distal accumulation of the plant growth regulator auxin (Aida et al., 2004; Blilou et al., 2005). Auxin distribution patterns have been linked with altered cell division planes during

embryo development (Petricka et al., 2009), lateral root initiation (Péret et al., 2009), and in primary roots (Sabatini et al., 1999). In addition, auxin accumulation in cultured cells alters PPB orientation and cell division planes (Dhonukshe et al., 2005). How auxin influences cell division planes and whether this directs stem cells and their daughters to divide in specific orientations has remained unknown.

Here, we show that PLT proteins induce root epidermal cells to orient cell division planes through TIR1-dependent auxin signaling (Dharmasiri et al., 2005a; Kepinski and Leyser, 2005), which enhances expression of microtubule-associated MAP65 proteins (Chan et al., 1999; Smertenko et al., 2000). MAP65 guides localization of CLASP, a microtubule cortex interaction mediator (Ambrose et al., 2011), and we postulate a mechanism by which this precisely orients cell division planes. Our results provide a paradigm for plant transcription factor control of cell division planes.

RESULTS

PLT1, PLT2, and PLT3 Are Required for LRC-Generating Periclinal Cell Divisions in the Root Stem Cell Niche

Arabidopsis root epidermis/LRC stem cells divide periclinally to generate new LRC layers and extend the epidermis by divisions perpendicular to the cell surface (anticlinal) (Figures 1A and Dolan et al., 1993). In roots of *plt1plt2* but not *plt3* and *plt1plt3* mutants, periclinal cell division frequency was reduced in the epidermis/LRC stem cell domain, whereas anticlinal divisions appeared normal (Figures 1C and 1L, and Table S1 available online). Consistent with periclinal cell division defects, *plt1plt2* roots possessed single or double LRC layers compared to three LRC layers in wild-type (WT) (compare Figure 1B with Figure 1C and compare the panels of Figure 1A), which did not occur in unrelated stem cell maintenance mutants (Figure S1F). In *plt1plt2* roots with a single outer layer, epidermis marker GL2::ER-GFP and epidermis/LRC marker WER::ER-CFP labeled the outer layer (Figures 1D and 1E, and Figures S1B–S1E) indicating a mixed identity. More *plt1plt2* but not *plt1* or *plt2* embryos revealed periclinal cell division defects (Figures 1F–1H) suggesting redundant roles for PLT1 and PLT2 in this process. The absence of periclinal epidermal divisions in *plt1plt2plt3* embryos (Galinha et al., 2007) indicated a residual role for PLT3 in this process. Indeed, *PLT3* coding region fused to the glucocorticoid receptor (GR) under the *PLT2* promoter restored periclinal cell divisions after DEX induction in the epidermis/LRC stem cell domain of *plt1plt2* roots, albeit to a lesser extent than the PLT2 coding region (Figures 1I–1J, 1L and Figure S1G).

Ectopic Induction of PLT1 and PLT2 Triggers LRC-Generating Periclinal Cell Divisions in the Root Epidermis

Induction of PLT2-GR or PLT1-GR from the constitutive 35S promoter in *plt1plt2* rescued periclinal divisions and, in addition, triggered periclinal cell divisions in the epidermis shootward from the stem cell niche (Figures 1K and 1L). In WT, constitutive induction of PLT1 or PLT2 triggered periclinal cell divisions throughout the root epidermis, leading to an extra layer (Figures 1M–1P and Figures S1H–S1I and S1O–S1P). Although cortex and endo-

dermis identity markers were unaltered after PLT2 induction, both daughter cells of periclinal cell divisions retained epidermal identity (Figure S1N). The LRC marker SMB (Figure 1Q), required for LRC differentiation (Bennett et al., 2010; Willemsen et al., 2008), appeared in the epidermis after induction of PLT2 (Figures 1Q and 1R) before periclinal cell division and asymmetrically segregated into outer daughter cells (see inset in Figure 1R) as in epidermis/LRC stem cells (see inset in Figure 1Q); these outer cells detach like typical LRC cells (Figure 1S). We concluded that PLT-induced ectopic periclinal cell divisions switch division planes and segregate cell fates similar to epidermis/LRC stem cells.

Dosage-Dependent and Cell-Autonomous PLT2 Action Switches Cell Division Planes

PLT proteins form gradients (Galinha et al., 2007), and periclinal divisions occur in the stem cell niche where PLT levels are elevated. The frequency of periclinal cell divisions increased with longer PLT2 induction times (Figures S1J–S1L) and PLT2::PLT2-YFP fusion proteins displayed strongest fluorescence in the stem cell niche region (Figure S1Q), indicating that high levels of PLT2 trigger periclinal cell divisions. Epidermal cells expressing higher PLT2 levels preferably underwent periclinal cell divisions, whereas neighboring cells with lower levels underwent anticlinal cell divisions (Figures 1T–1U and 1Y). We induced PLT2-YFP using the WER::XVE epidermis-specific induction system (A.P. Mähönen et al., in preparation), which triggered epidermal periclinal cell divisions (Figures S1R and S1S) strictly correlated with fluorescence-inferred expression strength based on serial scans (Figures 1V, 1W, and 1Z and Figures S1T and S1U). In six cell pairs within different roots, cells with higher PLT2-YFP levels before division underwent periclinal cell divisions, whereas neighboring cells with lower PLT2-YFP levels executed anticlinal cell divisions (Figure 1X). Together, our results indicate that PLT2 action promotes periclinal divisions in a dose-dependent and cell-autonomous manner.

Auxin and PLETHORA Together Trigger Periclinal Cell Divisions

In WT, auxin activity sensor DR5 built up in the epidermis/LRC stem cell prior to periclinal division and segregated asymmetrically in the outer daughter cell adopting LRC fate (Figures 2A–2C). After PLT2 induction, DR5 signal appeared in epidermal cells prior to periclinal cell division (Figures 2D and 2E). To address whether buildup of auxin levels was sufficient for periclinal divisions, we performed single-cell laser ablations (Sabatini et al., 1999; Xu et al., 2006), which block polar auxin transport. In the epidermis, cells rootward but not shootward of the ablated cell gradually accumulated DR5 signal (Figures 2F and 2G), and these cells divided periclinally (Figures 2F–2H).

The auxin efflux inhibitor 1-N-Naphthylphthalamic acid (NPA) also triggered DR5 increase and periclinal cell divisions mainly in the epidermal cells (Figures 2I and 2J and Figure S2). After NPA treatment, PLT expression increased in epidermal cells undergoing periclinal cell divisions (Figures 2K–2M). The ratio of NPA treated to untreated periclinal cell division frequency was higher in WT than that in *plt1plt2* mutant
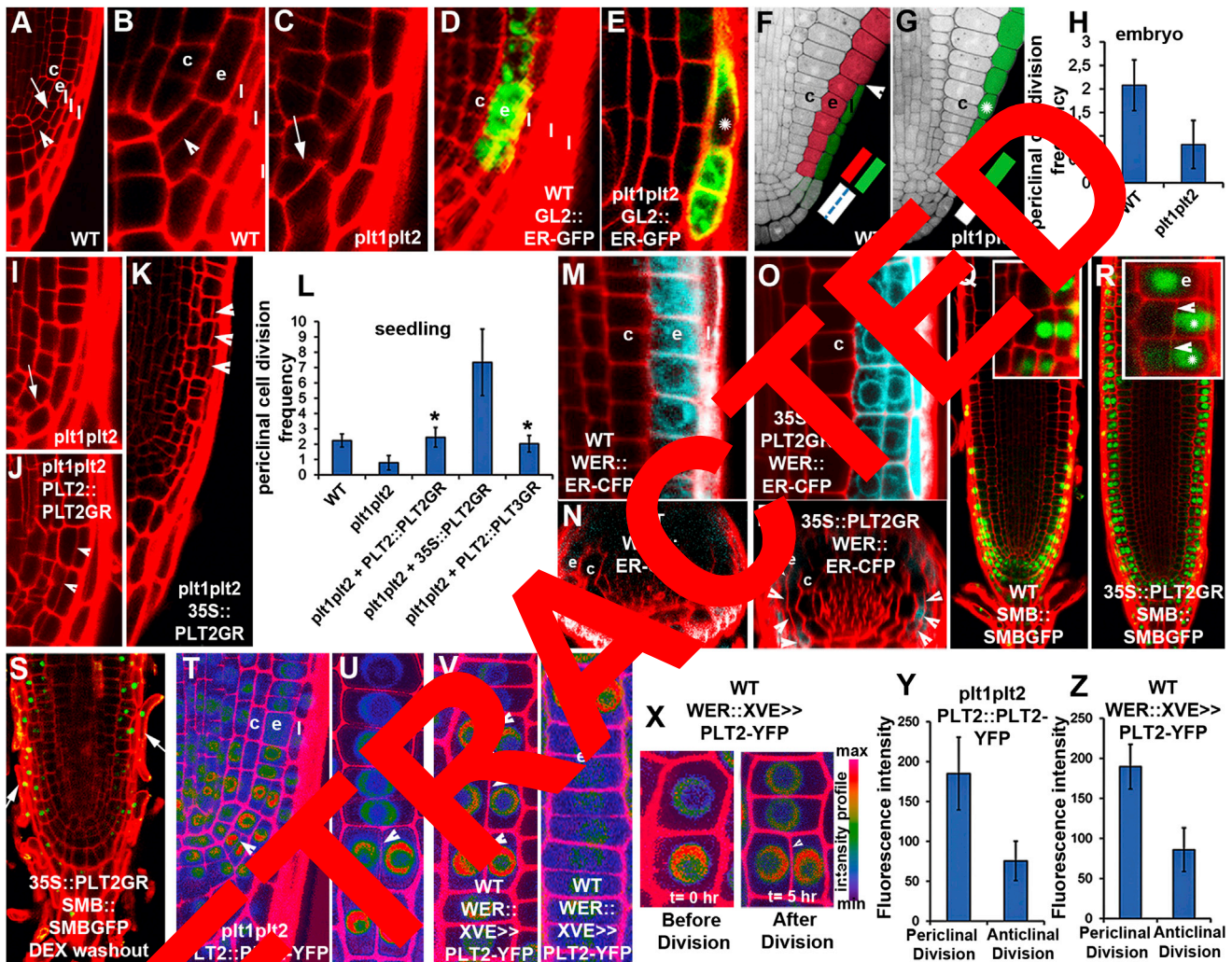
Figure 1. PLT Proteins Promote Periclinal Cell Divisions of Epidermis/LRC Stem Cells

(A) First periclinal cell division (white arrowhead) generates LRC and second anticlinal cell division (white arrow) extends epidermis in WT.

(B and C) plt1plt2 mutant with anticlinal cell division at position of periclinal cell division in WT (compare C with B). Note three LRC layers in WT (B) compared to one LRC layer in plt1plt2.

(D and E) Epidermis marker GL2::ER-GFP labels epidermis in WT (covered by three LRC layers D), and outermost layer in plt1plt2 (white asterisk in E).

(F–H) Aniline blue staining of WT (F) and plt1plt2 (G) mature embryos. WT with epidermis and LRC layers formed by periclinal cell divisions and single layer (white asterisk) in plt1plt2. Frequency of periclinal cell divisions in plt1plt2 (H).

(I–K) Periclinal cell divisions after induction of PLT2 (20 hr DEX) (compare I and J) and PLT3 (20 hr DEX; L and Figure S1G) in PLT2 domain. Ubiquitous PLT2 induction (20 hr DEX) in plt1plt2 induces periclinal cell divisions in extended epidermal regions (K).

(L) Periclinal cell division frequency in various analyzed backgrounds.

(M–P) Ubiquitous induction of PLT2 (24 hr DEX) triggers periclinal cell divisions in epidermis. Cross sections display the resulting extra cell layer (Compare N and P).

(Q and R) LRC marker SMB (Q) appears in the epidermis at the onset of periclinal cell divisions (R) and after cell division segregates in the outer layer (inset in R) adapting LRC fate.

(S) Detachment of outer layer expressing SMB (white arrows).

(T–Z) Amount of functional PLT2::PLT2-YFP in plt1plt2 correlates with periclinal cell division (fluorescence intensity quantification in Y and intensity profile analysis in T and U). Fluorescence intensity quantification in (Z) and intensity profile analysis in (V), (W), (X) correlate with higher PLT2 levels before periclinal divisions. White arrowheads depict periclinal cell divisions; white arrows mark anticlinal cell divisions. The following abbreviations are used throughout all figure legends: c, cortex; e, epidermis; and l, LRC. Red, propidium iodide (PI) staining; green, GFP; and cyan, CFP. Columns in graphs display means ; error bars, standard deviations; asterisk (*), statistically significant p values at < 0.05. n = 38 embryos for (H), n = 38 roots for (L), n = 23 cells from six roots for (Y) and n = 42 cells from nine roots for (Z) from three independent experiments. See also Figure S1.

(Figure 2N; compare with Figure 1L) indicating that NPA action to induce periclinal divisions requires *PLT* activity. The residual induction of NPA-triggered periclinal divisions in *plt1plt2* may either result from auxin-independent action on periclinal division or from enhanced activity of auxin-inducible PLT3 (De Smet et al., 2008).
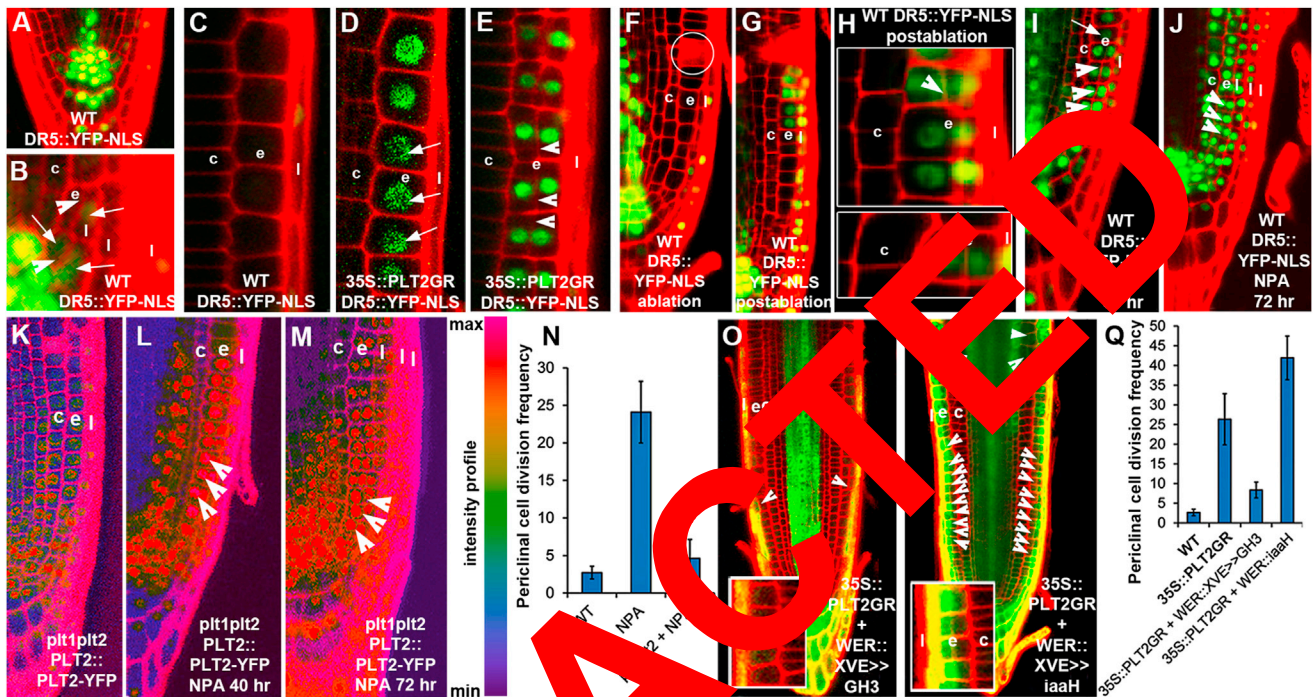
Figure 2. PLT2 Induced Periclinal Cell Division [is] Forecast by Auxin Activity and Require an Auxin Threshold

(A–C) DR5::YFP-NLS segregation after periclinal epidermis/LRC stem cell division (white arrows in B; n = 9 roots) and its restricted localization to LRC (C).

(D and E) Post-PLT2 induction (12 hr DEX treated [white arrows in D]) DR5::YFP-NLS appearance in epidermis prior to periclinal cell divisions (22 hr DEX treated [white arrowheads in E]).

(F–H) Laser ablation of epidermal cell (white circle in F and 24 hr after ablation G) triggers DR5::YFP-NLS appearance in epidermal cells below the ablated cell followed by periclinal cell division (G and H). (n = 12 ablated roots followed in three independent experiments).

(I and J) DR5::YFP-NLS appearance (white arrow in I) and periclinal cell divisions (white arrowheads in I) in the epidermis after NPA treatment. DR5::YFP-NLS in a premitotic cell (white arrow in I). Buildup of DR5::YFP-NLS from the root tip toward the root base correlating with periclinal cell divisions (J).

(K–N) Expression of PLT2-YFP in control and induced expression of PLT2-YFP and periclinal cell divisions (white arrowheads in L and M) after NPA-treatment. Frequency of NPA induced periclinal cell divisions in *plt1plt2* mutant (N).

(O and P) GH3-mediated auxin conjugation in epidermis (O) reduces PLT2 mediated periclinal cell divisions. Auxin overproduction by epidermal expression of iaaH (P) enhances PLT2 mediated periclinal cell divisions. After auxin overproduction some cortex cells also divide periclinally (P). DR5::ER-GFP levels correlate with efficiency of periclinal cell divisions (O and P).

(Q) Quantification of periclinal cell division frequency after PLT2 induction and auxin level manipulations.

Unless stated otherwise white arrowheads depict periclinal cell divisions and white arrows auxin activity as visualized by the DR5 reporter. Red, propidium iodide (PI) staining; green, GFP or YFP. Columns in graphs display means and error bars depict standard deviations. n = 29 roots for (N) and n = 28 roots for (Q) from three independent experiments. See also Figure S2.

We probed the role of local auxin abundance by expressing the auxin conjugating enzyme GH3.5 (Staswick et al., 2005) and the bacterial auxin synthesis gene iaaH (Kares et al., 1990) in the epidermis using the WER::XVE system. Coinduction of GH3.5 and PLT2 lowered DR5 signal in the epidermis, consistent with increased auxin conjugation, and reduced the frequency of periclinal cell divisions (Figures 2O and 2Q). In contrast, simultaneous iaaH and PLT2 induction enhanced DR5 signal in the epidermis and increased the frequency of periclinal cell divisions (Figures 2P and 2Q). Together, these results indicate that auxin levels influence cell division plane switch both through and in parallel to PLT action.

PLT2 Induces Periclinal Cell Division through TIR1-Dependent Auxin Signaling

The *tir1-1afb2-1afb3-1* triple auxin signaling mutant (Dharmasiri et al., 2005b) displayed periclinal cell division deficiencies

and abnormal cell division planes in the region where epidermis/LRC periclinal cell divisions normally occur (Figures 3A–3D). Strikingly, induction of PLT2 in *tir1-1afb2-1afb3-1* mutant increased root meristem size by triggering anticlinal cell divisions (Figures 3E, 3F, and 3O and Figures S3A–S3B). However, periclinal divisions were drastically reduced (Figures 3E, 3F, and 3N). We concluded that the TIR1 signaling pathway operates upstream of the PLT proteins for the general stimulation of cell division but downstream of the PLT proteins for triggering periclinal cell divisions. PLT2 induction in plants treated with the TIR1 signaling antagonist α-(phenyl ethyl-2-one)-indole-3-acetic acid (PEO-IAA) (Hayashi et al., 2008) also enhanced root meristem cell number, yet no DR5 appeared in the epidermis and very few periclinal cell divisions occurred (Figures 3H–3J and 3N and Figures S3E–S3F) in contrast to treatment with an inactive PEO-IAA analog (Figures 3K–3N and Figures S3C–S3D). NPA-induced
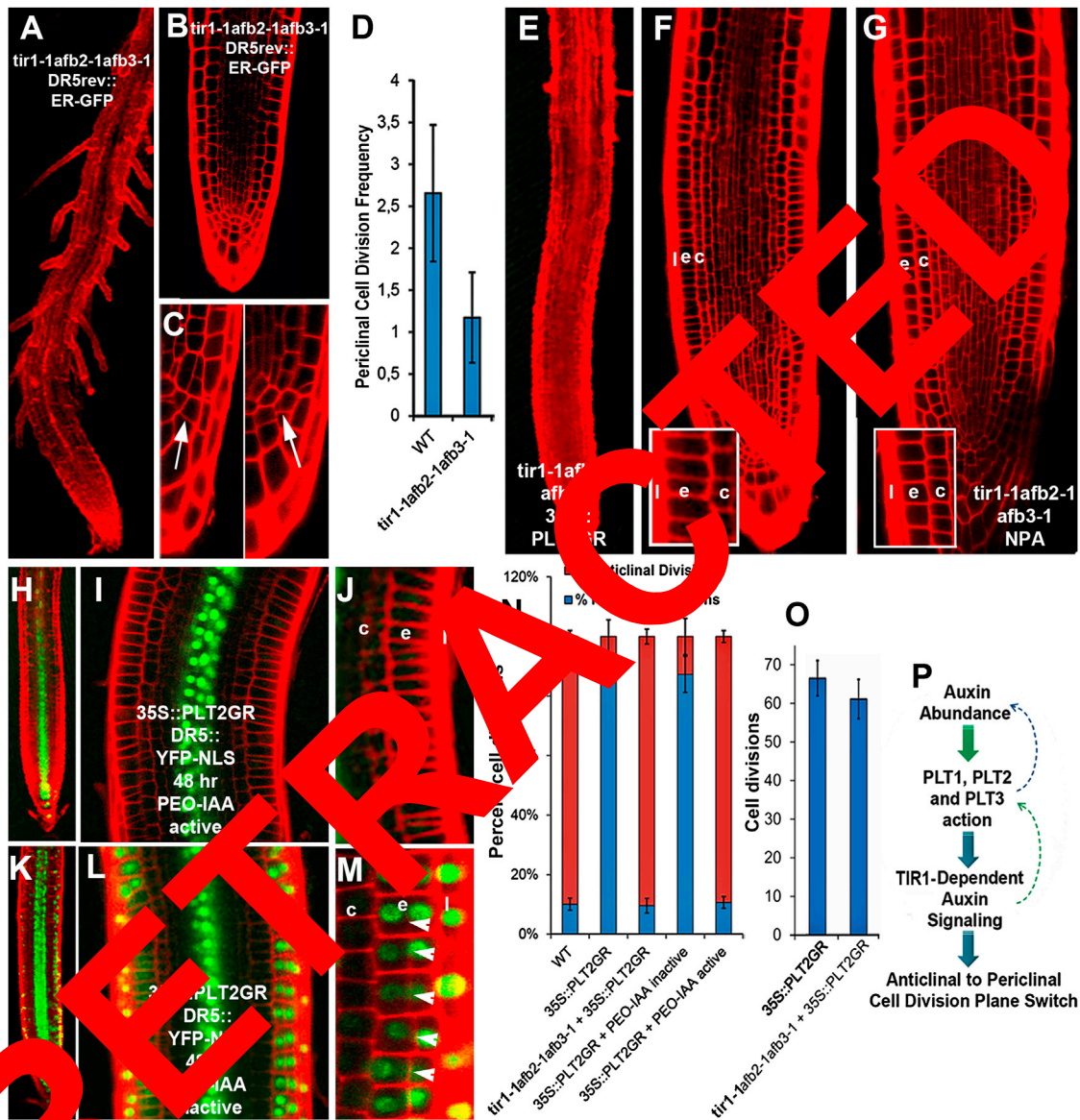
Figure 3. TIR1-Dependent Auxin Signaling Is Critical for PLT2 Induced Periclinal Cell Divisions

(A–D) *tir1-1afb2-1afb3-1* auxin signaling mutant with reduced meristem size (A and B), cell division plane defects (C), and reduced periclinal cell divisions (D) in epidermis/LRC layer cells.

(E–O) PLT2 induction rescues anticlinal (O) but not periclinal (N) cell divisions in *tir1-1afb2-1afb3-1* with increased root meristem size (compare E with A and F with B). NPA induced anticlinal but not periclinal cell divisions in *tir1-1afb2-1afb3-1* (G and N). Reduction of PLT2-mediated periclinal cell divisions in presence of auxin signaling antagonist PEO-IAA (H–J and N) but not in presence of the inactive analog PEO-IAA (K–N). Absence of DR5 signal in epidermis after PEO-IAA treatment (H–J) correlates with specific inhibition of periclinal cell divisions. Quantification of periclinal cell division frequencies and percentage periclinal and percentage anticlinal cell divisions (N).

(P) Summary of regulatory interactions. PLT induced periclinal cell divisions require auxin threshold and act through TIR1-dependent auxin signaling. PLT regulates auxin abundance and is auxin responsive. PLT expression is TIR1-auxin signaling pathway dependent. Blue arrows indicate interactions identified in this work, green arrows, previously published interactions.

White arrowheads depict periclinal cell divisions; white arrows mark anticlinal cell divisions. Red: propidium iodide (PI) staining and green: YFP. Columns in graphs display means and error bars depict standard deviations. n = 28 roots for (D), n = 29 roots for (N) and (O) from three independent experiments. See also Figure S3.

periclinal cell divisions were also drastically reduced in *tir1-1afb2-1afb3-1* mutant (Figure 3G) and after active PEO-IAA treatment (Figure S3G). Together our results reveal that TIR1-mediated auxin signaling is critical for stimulation of periclinal cell divisions by the PLT-auxin module (Figure 3P).
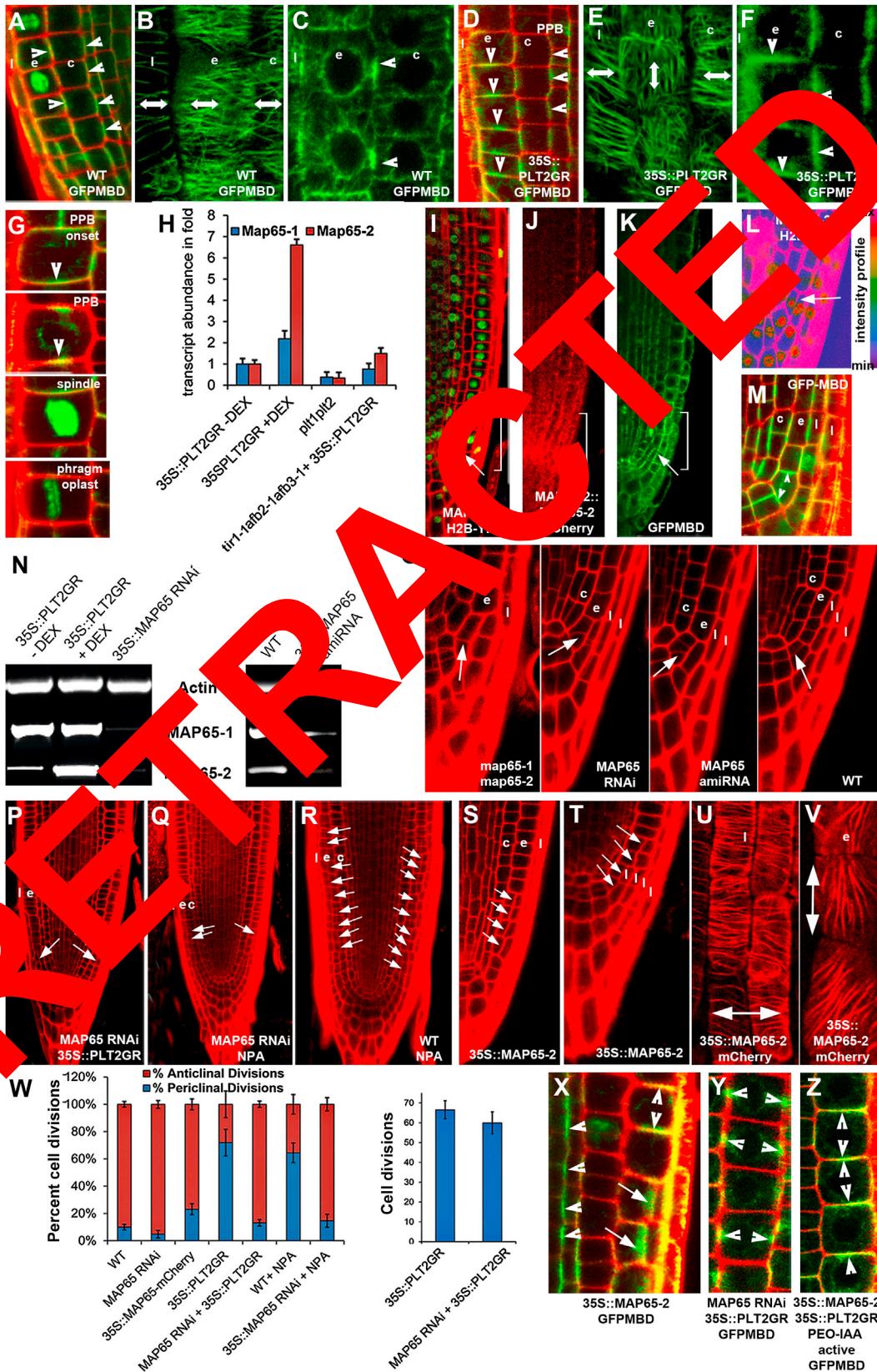
PLT Proteins Induce Premitotic Microtubule Reorganization and Cell Division Plane Switch through Transcriptional Regulation of MAP65-1 and MAP65-2

In WT epidermis, the PPB visualized by the GFP-microtubule binding domain (MBD) marker (Granger and Cyr, 2001) formed anticlinally and cells divided in that plane to extend the epidermis (Figures 4A–4C). However, after PLT2 induction, premitotic microtubules reorganized longitudinally and formed periclinal PPBs (Figures 4D–4F), forecasting the periclinal cell division plane (Figure 4G). As a transcription factor, PLT2 should switch cell division plane through its transcriptional targets. We pursued downstream targets of PLT2 by a genome-wide microarray analysis that distinguished between direct and indirect targets (R. Heidstra and B. Scheres, in preparation). This analysis suggested that plant microtubule-associated protein MAP65-2 (Li et al., 2009) was upregulated by PLT2. qRT-PCR analysis confirmed that *MAP65-2* is upregulated by PLT2 prior to PLT2-mediated induction of periclinal cell division (Figure 4H). The closely related *MAP65-1* (Smertenko et al., 2008) was also induced by PLT2 (Figure 4H). In *tir1-1afb2-1afb3-1* mutants, PLT2 did not efficiently induce *MAP65-1* and *MAP65-2* upregulation (Figure 4H), indicating that their induction requires TIR1-dependent auxin signaling. Transcriptional and translational *MAP65-2* fusions were strongly expressed in regions with longitudinal microtubules (Figures 4I–4M) where LRC-generating periclinal cell divisions occur. Our data agree with the *MAP65-2* mRNA profile of the *Arabidopsis* root (Brady et al., 2007), and indicate that *MAP65-2* transcript levels are regulated by the PLT gradient in the root.

Single *map65-2* and *map65-1* T-DNA insertion mutants (Figure S4A) did not display cell division plane defects in the epidermis/LRC domain (not shown). We obtained *map65-1map65-2* double mutants (Figure S4B) and repressed the expression of both genes by RNAi and amiRNAi approaches (Figure 4N). All lines exhibited similar decreased periclinal divisions and cell division plane alterations in the epidermis/LRC stem cell region, creating fewer LRC layers (Figure 4O). We

focused our analysis on MAP65 RNAi lines and found that PLT2 induction or NPA treatment in this background led to reduced periclinal cell division induction (Figures 4P, 4R, and 4W). Overexpression of MAP65-2 was sufficient to trigger cell division plane switches in epidermal cells proximal to the root stem cell niche (Figures 4S and 4W) and occasionally created an extra LRC layer (Figure 4T). Subsequently, we visualized the microtubule conformation in MAP65-2-overexpressing lines using MAP65-2-Cherry (Figures 4U and 4V), GFP-MBD (Figure 4X), or GFP-tubulin (Ueda et al., 1999; Figure S4C). Overexpression of MAP65-2 induced microtubule bundling (Figures S4C–S4E) and premitotic microtubules organized longitudinally in several MAP65-2-overexpressing epidermal cells, resulting in the formation of periclinal PPBs (Figures 4V and 4X). Induced PLT2 was unable to switch PPB position from anticlinal to periclinal in MAP65 RNAi lines (Figure 4Y), consistent with the notion that MAP65-1 and MAP65-2 operate downstream of *PLT* genes. In addition, auxin-signaling-independent constitutive *MAP65-2* expression allowed PPB relocation when PLT2 was induced with impaired auxin signaling (Figure 4Z). We concluded that MAP65-2 bypasses the requirement of TIR1 auxin signaling for PPB relocation and acts downstream of TIR1 auxin signaling. Our results show that MAP65-2 is a downstream effector of PLT2 auxin signaling action with the capacity to alter microtubule conformation, change PPB placement and reorient cell division planes.

PLT2 Induced Premitotic Microtubule Reorganization Depends on CLASP Function and CLASP Localization Is MAP65 Dependent

The *clasp-1* mutation in the microtubule bypass mediator CLASP (Ambrose et al., 2011) revealed cell division plane abnormalities in the epidermal/LRC stem cell division region (Figures 5A and 5C). PLT2 was unable to efficiently induce epidermal periclinal cell divisions in the *clasp-1* mutant (Figures 5B and 5D). A functional GFP-CLASP fusion expressed under the CLASP promoter that rescued the *clasp-1* mutant phenotype (Ambrose et al.,

---

Figure 4. PLT2 Triggers Premitotic Microtubule Organization Switch through TIR1-Dependent Transcriptional Regulation of MAP65-1 and MAP65-2

(A–C) GFP-MBD labeled microtubules in WT display transverse orientation (B) along with transverse PPBs (C) and anticlinal cell divisions (A).

(D–G) PLT2 induction triggers transverse to longitudinal pre-mitotic microtubule reorganization in epidermis (D and E), along with PPB orientation switch by 90° (F and G) and periclinal cell division (G).

(H) MAP65-1 and MAP65-2 levels after PLT2 induction in WT and *tir1-1afb2-1afb3-1* mutant (16 hr DEX). qRT-PCR expression values are from three independent experiments.

(I–M) MAP65-2 expression in stem cell niche. MAP65-2 expression is high in cells that can undergo periclinal cell divisions (white arrow in I, J, K, and L) where the microtubules localize to apical and basal cell sides (K) and form a periclinal PPB (white arrowheads in M). Zone marked by white brackets reveals gradual reduction in apical-basal microtubules marked by GFP-MBD correlated with reduced capacity to undergo periclinal cell divisions.

(N) RT-PCR analysis of MAP65-1 and MAP65-2 transcripts in MAP65-1MAP65-2 RNAi ('MAP65RNAi') and MAP65-1MAP65-2 amiRNA ('MAP65amiRNA') lines.

(O) Division plane changes and LRC reduction in *map65-1-1map65-2-1*, MAP65RNAi, and MAP65amiRNA lines. White arrows indicate cell division orientations.

(P–R) MAP65-1MAP65-2 silencing reduces NPA-triggered (compare Q and R) or PLT2-triggered periclinal cell divisions (P).

(S–V) MAP65-2 overexpression induces periclinal cell divisions in epidermis proximal to the stem cell niche. Note recent periclinal divisions (S) or extra LRC layer (T) indicating embryonic periclinal division (T). MAP65-2 labeled microtubules reorient in epidermal cells prior to periclinal cell division (V) but not in LRC cells (U). White arrows indicate periclinal cell divisions and bidirectional white arrows depict microtubule orientation.

(W) Quantification of periclinal and anticlinal cell division frequencies and number of cell divisions in MAP65-1- and MAP65-2-related manipulations. The columns in graphs display means and error bars represent standard deviations. n = 28 roots from three independent experiments.

(X–Z) GFP-MBD labeled microtubules mark periclinal PPB in MAP65-2 overexpression line (X). PLT2 induction after MAP65 repression does not switch PPB orientation from anticlinal to periclinal (Y). TIR1-auxin signaling-independent expression of MAP65-2 after PLT2 induction and PEO-IAA treatment switches PPBs to periclinal orientation (Z). White arrows indicate periclinal cell divisions, white arrowheads, PPBs.

Red, propidium iodide (PI) staining and green, GFP or YFP. See also Figure S4.
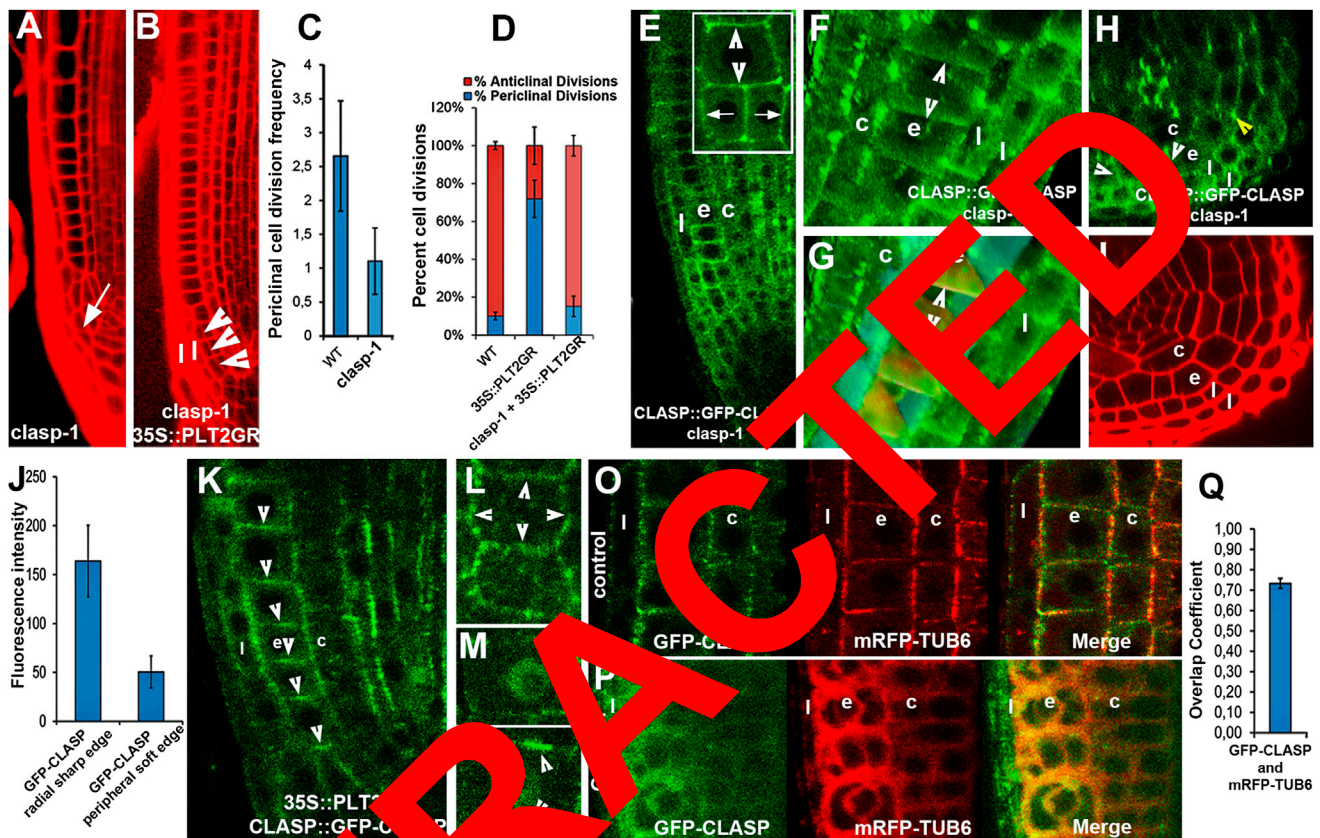
Figure 5. PLT2-Triggered Switch in Premitotic Microtubule Organization Requires CLASP Action and CLASP Localization Is Microtubule Dependent

(A–D) Abnormal cell division orientation in epidermis/LRC stem cell in *clasp-1* mutant (A) and reduced frequency of periclinal cell divisions (C). PLT2 induced periclinal cell divisions are reduced in *clasp-1* (B and D).

(E–J) GFP-CLASP labels apical-basal cell sides (white arrowheads) prior to division only in epidermis/LRC stem cells prone to undergo periclinal cell division, and lateral cell sides (white arrows) in divided epidermis/LRC stem cells and all other cells (E). 3D assembly of 30 0.5 µm equidistant CLSM scans depicts differential GFP-CLASP localization to apical-basal cell sides in epidermis/LRC domain cells prone to undergo periclinal cell division (F). Image is color coded to highlight different cell sides (G). Cross-sections with GFP-CLASP enrichment on radial cell sides (the cell sides on which a PPB assembles to mark a periclinal cell division) are evident by quantification of GFP-CLASP intensity at radial and peripheral cell edges (J).

(K–N) After induction of PLT2, CLASP labels apical-basal cell sides (white arrowheads) prior to division (K). During reorientation, GFP-CLASP displays transient nonpolar localization (L–N).

(O–Q) CLASP colocalization with tubulin-labeled microtubules (see the overlap coefficient in Q) and aberrant CLASP localization after oryzalin induced microtubule depolymerization (P).

White arrowheads depict periclinal cell divisions, white arrow anticlinal cell divisions in (A) and (B). Red, propidium iodide (PI) staining or mRFP and green, GFP. White arrowheads depict GFP-CLASP localization in (E)–(N). Graph columns depict means, error bars indicate standard deviation. n = 26 roots for (C), n = 29 roots for (D), n = 40 cells from 6 roots for (J) and n = 22 cells from five roots for (Q) from three independent experiments. See also Figure S5.

2011) was expressed in the root region encompassing formative cell divisions (Figure 5E). CLASP localized predominantly to apical and basal cell sides within the epidermal/LRC domain prior to periclinal cell divisions, in contrast to its lateral localization after periclinal division and in many other cell types undergoing anticlinal cell divisions (Figures 5E–5G). Furthermore, CLASP was enriched at sharp radial cell edges (Figures 5H–5J). This CLASP localization typically occurred within cells competent to undergo periclinal cell divisions (Campilho et al., 2006), but not in cells or cell layers where anticlinal cell divisions take place (Figures 5E–5G). PLT2 induction and NPA treatment gradually shifted CLASP localization from lateral to apical-basal

cell sides, consistent with the capacity of these manipulations to relocate PPBs (Figures 5K–5N and Figures S5A–S5F). CLASP abundance was not altered after PLT2 induction and auxin application (Figure S5G).

GFP-CLASP and mRFP-tubulin coexpression revealed CLASP colocalization with microtubules (Figures 5O and 5Q). Interestingly, CLASP lost its cell-edge-related localization after oryzalin-induced microtubule depolymerization (Figure 5P), demonstrating that the maintenance of subcellular CLASP localization requires intact microtubules.

PLT2 induction increased MAP65-1 and MAP65-2 expression in the *clasp-1* mutant (Figure S6E) but failed to induce periclinal

cell divisions indicating that CLASP and MAP65 are both required for microtubule array reorientation and cell division plane switch. To probe the nature of this interdependency we first analyzed whether localization and function of CLASP depends on MAP65 levels. MAP65-2 overexpression induced transverse microtubule bundles in cells within the epidermal/LRC region, which were colabeled with CLASP especially at the apical-basal cell edges (Figure 6A and Figures S4C–S4E). Quantitative fluorescence intensity profiling revealed selective enrichment of CLASP at microtubule bundles possessing higher MAP65 levels and contacting top-down cell edges (Figures 6C and 6F) and CLASP colocalization with MAP65 at these edges (Figure 6E). MAP65-positive microtubule bundles were relatively resistant to oryzalin-induced microtubule depolymerization (Figures S6A–S6D). CLASP retained its cell-edge-related localization where MAP65-positive microtubule bundle resisted microtubule depolymerization (Figures 6B, 6D, and 6G), suggesting that MAP65 reinforces CLASP persistence at cell edges. Indeed, CLASP did not efficiently load on microtubules and on cell edges in the MAP65 RNAi line and instead remained largely cytosolic (Figures 6L and 6M). The localization of CLASP at apical-basal cell sides was more severely affected than lateral cell sides (Figures 6L and 6M and compare Figure 5E with Figure 6L). Our data reveal that MAP65 has a role in recruiting CLASP on microtubules and at apical-basal sharp cell edges that promote microtubule passage at those edges to favor anticlinal PPB and periclinal cell divisions. Conversely, MAP65 induced many transverse and a few longitudinal microtubule bundles in the absence of CLASP (Figure 6O). Overexpressed CLASP induced microtubule bundles in nonroot cell types (Kirik et al., 2007), and in our hands also induced spaghetti-shaped microtubule bundles in root cells (Figure 6O) but did not consistently reorient cell division planes (Figures 6K–6N), although randomized cell division planes were occasionally observed (data not shown). Overexpressed CLASP was unable to load on to microtubules and induce microtubule bundling in the MAP65 RNAi line (Figures 6P and 6Q). Together our results show that MAP65 function is required for CLASP localization to microtubules, CLASP recruitment to the edges of apical-basal cell sides, and for CLASP function.

CLASP-Facilitated Crossing of Apical and Basal Cell Edges Is Sufficient for 90° Rotation of the Microtubular Array

In switching from an anticlinal to a periclinal cell division, the premitotic cortical microtubule array reorients and the orientation of the PPB changes by 90°. How can this orientation be so precisely controlled? It was recently shown that microtubule organization in nondividing cells is influenced by the ease with which microtubules can traverse edges between adjacent cell faces (Ambrose et al., 2011). We tested whether CLASP-induced changes in microtubule crossing rates at the cell edges bounding the apical and basal cell faces are sufficient to reliably switch the orientation of the microtubule array for rotating the cell division plane. To that end we performed simulations of interacting microtubules on cubical surfaces using a previously developed algorithm (Tindemans et al., 2010); see Extended Experimental Procedures for details).

The barrier presented by a cell edge for microtubule crossing to an adjacent cell face was modeled as a probability of undergoing a catastrophe upon reaching the edge, chosen differently for the periclinal edges (P_{PC}) and anticlinal edges (P_{AC}) (Figure 7A). Ambrose et al. (2011) have shown that in the absence of CLASP, anticlinal edges present a strong barrier to microtubule crossing, so we associated it with high values of P_{AC}. When CLASP localizes to anticlinal edges, microtubules readily cross to and from the apical and basal faces, which we associated with small values of P_{AC}. To quantify the orientation of the aligned array on the apical surface, we introduced an order parameter C_2 with value for a perfectly ordered array in an anticlinal orientation and value 1 for a perfectly ordered array in one of the equivalent final orientations. Figure 7A displays average values as a function of the catastrophe probability on impinging an anticlinal edge P_{AC} for systems with and without bundling. When $P_{AC} > P_{PC}$ (low density of CLASP at the anticlinal edges), microtubules attempting to cross experience a high rate of edge-induced catastrophes and hence have a diminished lifespan. In this case we find $C_2 \sim 1$, indicating that these systems are almost exclusively ordered with an anticlinal orientation. When $P_{AC} < P_{PC}$ (high density of CLASP at the anticlinal edges), the lifespan of microtubules entering the apical and basal surfaces is enhanced with respect to those attempting to cross over between periclinal faces, and we find $C_2 \sim -0.5$, indicating predominant periclinal ordering. This is illustrated by two characteristic snapshots taken at a high value of P_{AC} (Figure 7B) and a low value of P_{AC} (Figure 7C). In the intermediate regime where $P_{AC} \sim P_{PC}$ the ability of the system to choose a specific orientation was impaired. This resulted in bimodal distributions for the order parameter C_2 (see Figure S7), indicating that the system randomly chooses one of the three possible orientations dictated by the symmetry of the cell. We also addressed the role that MAP65-mediated bundling could play in this process. Histograms of the order parameter C_2 for the four possible situations in presence or absence of CLASP, and presence or absence of bundling, revealed that in all cases a unique anticlinal (Figures 7D and 7F) or periclinal (Figures 7E and 7G) orientation is obtained. Our simulations reveal that changes in CLASP positioning are sufficient to reliably determine emergent 90° switches in orientation of the microtubule array. The simulations further suggest that the role of MAP65 in cell division plane orientation is primarily through its contribution to CLASP localization rather than microtubule bundling.

DISCUSSION

Spatiotemporal Control of Formative Divisions

In this study we show that PLT transcription factors and auxin together control the division plane reorientation and asymmetric cell division that defines a formative division in plants. The PLT proteins and the auxin response machinery upregulate members of the MAP65 family of microtubular cytoskeleton regulators, which we show to be essential for premitotic microtubule array reorientation and cell division plane rotation through a hitherto unexpected role in CLASP localization. Our work thus addresses the long-standing issue of how patterning is connected to the mechanistic control of precisely oriented cell divisions in plants.
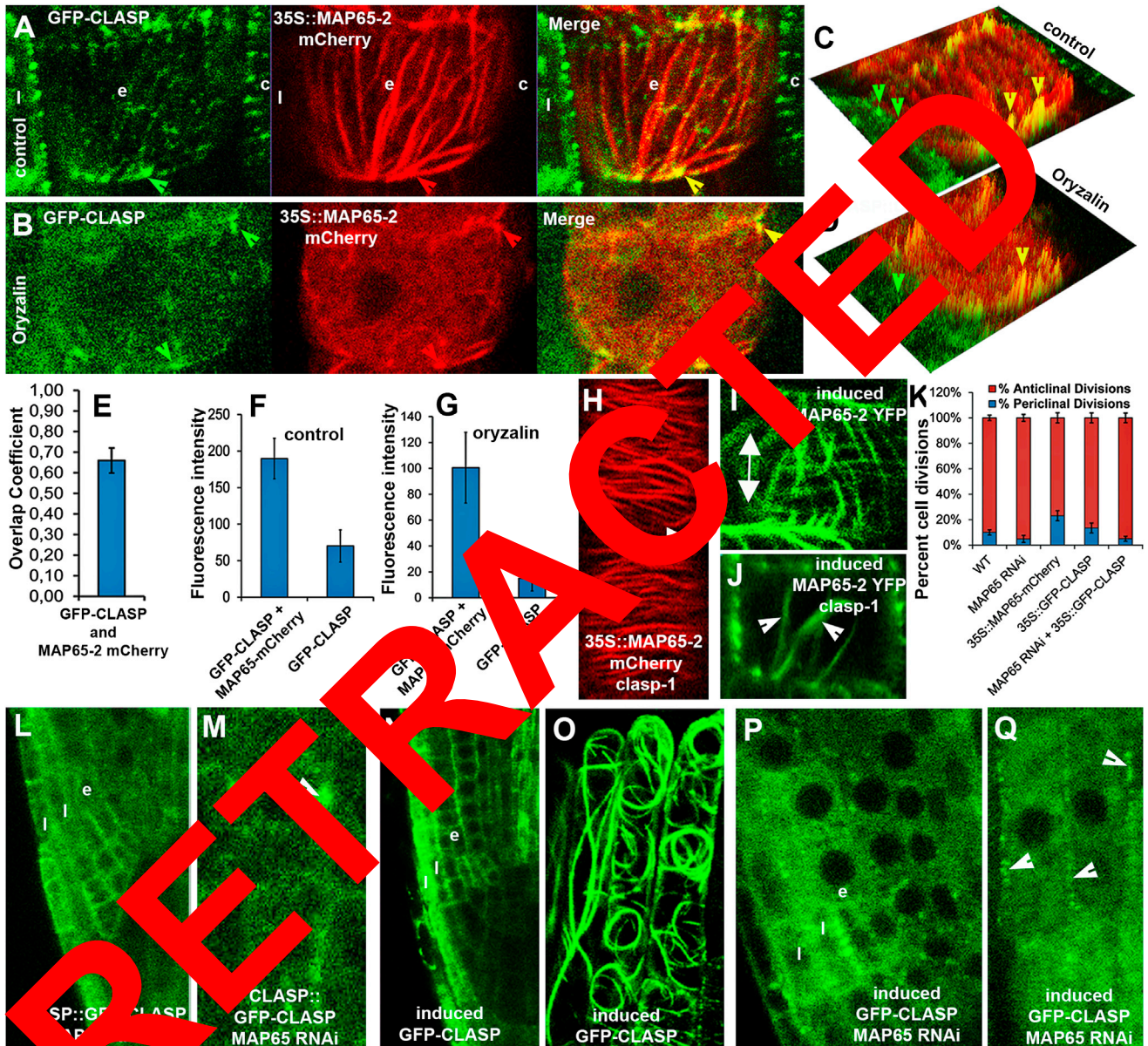
Figure 6. CLASP Localization to Microtubules and to Apical-Basal Cell Sides Require MAP65

(A–G) CLASP colocalizes with MAP65 on microtubules (overlap coefficient in E). Overexpressed MAP65 induces microtubule bundling and retains CLASP on oryzalin resistant longitudinal microtubule bundles. Full intensity profile landscapes of whole images shown in C and D. CLASP intensity (green peaks highlighted by green arrowheads in C) on transversal microtubules in MAP65-2 mCherry nonexpressing cell is reduced compared to longitudinal microtubules in neighboring cell expressing MAP65-2 mCherry (yellow arrowheads in C). After oryzalin treatment green-colored CLASP intensity in the cell without overexpressed MAP65 decreases (green arrowhead in D), but colocalization with red MAP65-2 intensity peaks (yellow arrowhead in D) remains in cell overexpressing MAP65-2 mCherry. GFP-CLASP intensity quantification shown in (F) and (G).

(H–J) MAP65 microtubule localization and bundling capacity is CLASP-independent both after constitutive (H) and induced expression (J). In WT, induced MAP65 triggers formation of more longitudinal microtubule bundles and transverse-to-longitudinal microtubule array switch (I), whereas in absence of CLASP its efficiency to induce longitudinal microtubule bundles (compare J with I) and microtubule array reorientation (H) is hampered.

(K) Quantification of periclinal and anticlinal cell division frequencies in case of MAP65 and CLASP overexpression.

(L and M) CLASP localization to microtubules, especially to longitudinal microtubules (compare L with Figure 5E), is impaired upon MAP65 repression.

(N–Q) CLASP promotes microtubule bundles but less after MAP65 repression (compare N and O with P and Q), which promotes predominant cytosolic localization of CLASP.

Bold bidirectional arrows show direction of microtubule orientation. White or green arrowheads indicate GFP-CLASP localization and red arrowheads depict MAP65-mCherry. The columns in graphs display means, and error bars represent standard deviation. n = 34 cells from five roots for (E), n = 45 cells from eight roots for (F), n = 37 cells from eight roots for (G) and n = 29 roots for (K) from three independent experiments. See also Figure S6.
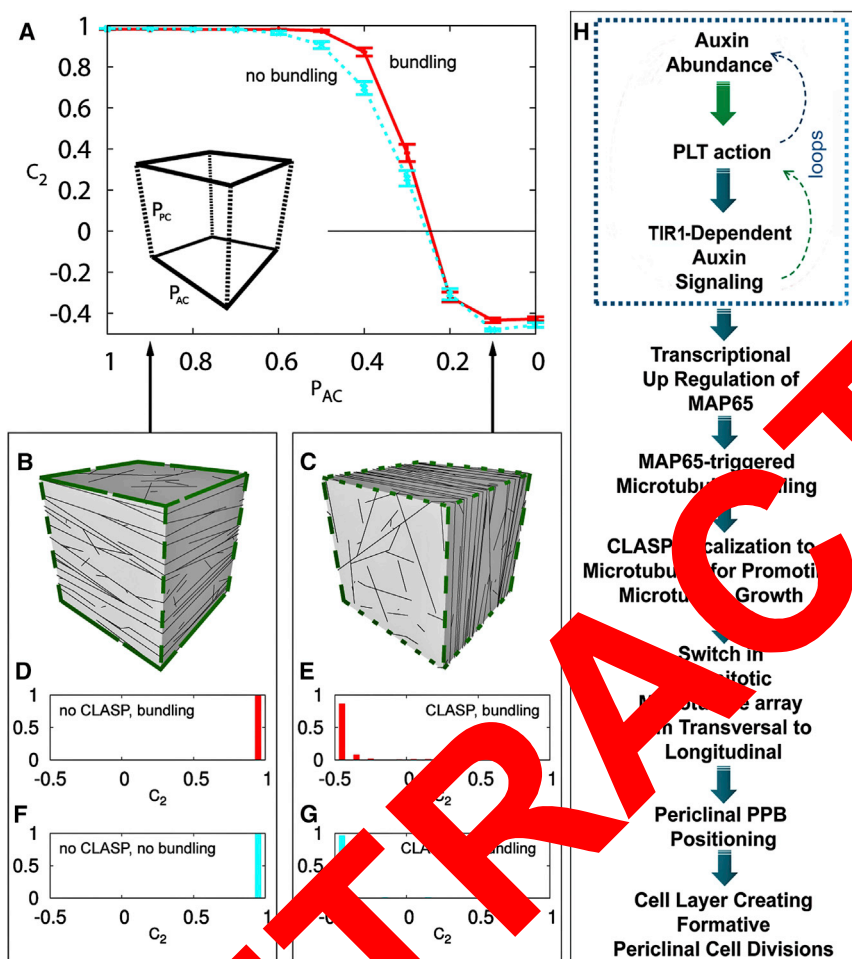
Figure 7. A Model for Transcription-Factor-Mediated Precise Rotation of Cell Division Plane

(A–E) Impact of CLASP-based differences in catastrophe probability when crossing cell edges determine stochastic simulations of interacting cortical microtubules. Spontaneous catastrophe probability for microtubules crossing an edge given by P_{AC} (anticlinal edges) and P_{PC} (periclinal edges), subscript. P_{AC} decreased from 1 to 0 with $P_{PC} = 0.26$ constant. When the anticlinal edges are hard or impossible to cross, a transverse orientation prevails (Alignment order parameter C_2, with a maximum of $C_2 = 1$ when microtubules are transversely aligned). When the anticlinal edges are easiest to cross, the longitudinal alignment dominates ($C_2 < 0$, with a minimum of $C_2 = -0.5$ when all microtubules are longitudinally aligned). This holds true both with (red solid curve) and without (cyan dotted curve) microtubule bundling. Both curves cross $C_2 = 0$ when $P_{AC} \sim P_{PC}$, i.e., when there is no appreciable difference between anticlinal and periclinal edges.

Bottom panels present two specific cases: without CLASP located at the anticlinal edges (left; $P_{AC} = 0.9$) and with CLASP at the anticlinal edges (right; $P_{AC} = 0.1$). Snapshots (B) and (C) show representative microtubule arrays for WT cells, i.e., with bundling. The superimposed green lines show the ease of crossing the edge: easy (dotted, $P_{AC} = 0.1$), intermediate (dashed, $P_{PC} = 0.26$) and hard (long dashed / almost solid, $P_{AC} = 0.9$).

Histograms of array orientations (N = 200 simulations each) for the same parameters are shown in (D) and (E), respectively. Histogram (F) corresponds to the MAP65 mutant, which has neither bundling nor CLASP at the anticlinal edges. (G) represents a hypothetical MAP65 mutant deficient in bundling, but allowing proper CLASP localization at the anticlinal edges.

(H) Summary of regulatory interactions: The PLT2-auxin pathway changes abundance of MAP65, which facilitates CLASP relocalization for cell division plane switching. Blue arrows, the interactions identified by this work; green arrows, previously published interactions.

See also Figure S7.

The epidermis/LRC formative cell division takes place repeatedly in the stem cell niche of the *Arabidopsis* root, where PLT proteins are abundant (Galinha et al., 2007) and where the growth regulator auxin reaches maximum levels (Grieneisen et al., 2007; Petersson et al., 2009). Auxin signaling is required for the initiation of PLT transcription (Aida et al., 2004), but PLT transcriptional activation also induces increased auxin response (Galinha et al., 2007; this manuscript). Both high PLT activity and threshold auxin levels promote the epidermis/LRC formative division. This synergy between high PLT levels and auxin action on the epidermis/LRC division may serve to precisely specify the position of formative divisions. The auxin signaling TIR1 module is critically required for the execution of division plane rotation downstream of PLT gene action but upstream of MAP65 activation. This pathway suggests that PLT action activates specific auxin responsive transcription factors (ARFs) or represses their repressors (AUX/IAAs) (Guilfoyle and Hagen, 2007; Lau et al., 2011) to allow a specific change in auxin response leading to

MAP65 transcription. Similar adaptive changes in auxin response factors have been demonstrated for the progression of lateral root initiation (De Smet et al., 2010). The notion of specialized auxin response modules for cell division plane regulation is consistent with reports on precise alterations in cell division planes upon reduction of ARF function in the embryo (Hamann et al., 1999; Hardtke and Berleth, 1998). Intriguingly, PLT expression in the *tir1-1afb2-1afb3-1* auxin signaling mutants uncouples control of cell division orientation from the general stimulatory effect of auxin on cell division. In contrast, PLT induction in lines with reduced ABP1 activity, which represents another auxin signaling pathway, could not rescue general cell cycle control (Tromas et al., 2009).

Microtubule-Based Division Plane Control in Multicellular Context

We demonstrate that MAP65 and CLASP proteins, involved in microtubule dynamics, are relevant players in the control of the

epidermis/LRC stem cell formative division and the associated shift in PPB positioning. MAP65-1 and MAP65-2 localize to regions of microtubule overlap and promote crosslinking of anti-parallel microtubules and their stabilization (Gaillard et al., 2008; Li et al., 2009; Van Damme et al., 2004). Recent dynamic coloc-alization of MAP65-1 and MAP65-2 with polymerizing microtu-bules indicate that plant cortical microtubules bundle through a microtubule-microtubule templating mechanism (Lucas et al., 2011). Another member of the same MAP65 protein family, MAP65-4, promotes microtubule bundle elongation (Fache et al., 2010). However, we show that the role of MAP65 in division plane reorientation may be separable from microtubule bundling and instead largely relies on its role in CLASP localization.

Plant CLASP and MAP65 proteins have both been implicated as regulators of general microtubular array stability (Ambrose et al., 2011; Kirik et al., 2007; Li et al., 2009). In addition, there is evidence that CLASP increases the attachment strength of microtubules to the cell cortex (Ambrose and Wasteneys, 2008). CLASP levels are not regulated by PLTs or auxin and CLASP is expressed ubiquitously in mitotic root cells (Kirik et al., 2007). CLASP's involvement in selective microtubule passage at sharp cell edges (Ambrose et al., 2011) and apical localization at those edges during the cell division plane switch (this study) suggest that localized CLASP guides directional microtubule reorganization. How CLASP is recruited to specific cell edges remains unclear, but MAP65 plays a role in either delivery by microtubules or stabilization of CLASP at selected cell edges and then, through its association with transfacial microtubule bundles, enables the passage of microtubules. Our modeling efforts support a scenario in which localization of CLASP by MAP65, rather than MAP65 bundling activity, contrib-utes to cell division plane switching. The simulations reveal that CLASP localization to anticlinal edges, enabling microtubules to freely pass, is a robust mechanism for precisely switching the preferred orientation of the cortical array. As presence or absence of microtubule bundling without considering CLASP function has little effect on this mechanism, MAP65 likely facili-tates the process through its role in CLASP localization.

It is broadly recognized that the cortical microtubule array is a self-organizing network where microtubule nucleation, dynamic microtubule growth and microtubule-microtubule encounters determine spatial ordering (Wasteneys and Ambrose, 2009). Our results demonstrate how transcription factors feed into cytoskel-etal dynamics through MAP65-mediated CLASP localization. The precise cellular mechanisms by which CLASP is differentially localized and how this affects microtubule dynamics will have to be elucidated in future studies.

EXPERIMENTAL PROCEDURES

Plant Material and Microscopy

Details of plant lines and growth conditions, constructs, molecular cloning, plant transformation, and expression profiling are described in Supplemental Information. Confocal laser-scanning microscopy (CLSM) (Dhonukshe et al., 2006; Dhonukshe et al., 2008) and cell ablations (Xu et al., 2006) were per-formed as previously described. Fluorescence signal intensity was analyzed with Leica (Live) and Zeiss (ZEN) confocal softwares. Overlap coefficients were calculated based on Manders et al. (1992). Data were statistically evalu-ated with Excel 2003 (Microsoft). Cell surface and median confocal sections

displaying microtubules were obtained with slightly widened pin-holes in the CLSM setup that allows visualizing microtubule conformations in cells within the same confocal section.

Chemical Treatments

NPA (Duchefa), Oryzalin (Sigma), Dexamethasone (Sigma), Estradiol (Sigma), and PEO-IAA (a gift from Prof. Hayashi) were used from DMSO stock solutions at 25 μM NPA, 2 μM Oryzalin, 10 μM Dexamethasone (Dex), 5 μM Estradiol, and 20 μM PEO-IAA working concentrations as indicated in Methods.

Cell Division Plane Frequency Analysis

Periclinal cell division frequency in the epidermal layer including the epidermis/LRC stem cell region (the green region in Figure S1M) was quantified by counting periclinal cell divisions in comparable CLSM root scans. Periclinal and anticlinal division ratios were obtained by counting the number of peri-clinal and anticlinal cell divisions and dividing by total division number from the colored regions as shown in Figure S1M. plt1plt2 and tir1-1afb2-1afb3-1 mutants had very short roots so only the periclinal cell division was quantified. Upon rescue of cell divisions after PLT2 induction in those mutants al-lowed quantification of periclinal and anticlinal cell division ratios. Data were statistically evaluated with Excel 2003 (Microsoft).

Computer Simulations

The simulations of the cortical microtubule array were performed using the event-based algorithm also employed in Tindemans et al. (2010). Details are described in the Supplemental Information.

SUPPLEMENTAL INFORMATION

Supplemental Information includes Supplemental Experimental Procedures, seven figures, and one table and can be found with this article online at doi:10.1016/j.cell.2012.02.051.

REFERENCES

Aida, M., Beis, D., Heidstra, R., Willemsen, V., Blilou, I., Galinha, C., Nussaume, L., Noh, Y.S., Amasino, R., and Scheres, B. (2004). The PLETHORA genes mediate patterning of the Arabidopsis root stem cell niche. Cell 119, 109–120.

Allard, J.F., Wasteneys, G.O., and Cytrynbaum, E.N. (2010). Mechanisms of self-organization of cortical microtubules in plants revealed by computational simulations. Mol. Biol. Cell 21, 278–286.

Ambrose, J.C., and Wasteneys, G.O. (2008). CLASP modulates microtubule-cortex interaction during self-organization of acentrosomal microtubules. Mol. Biol. Cell 19, 4730–4737.

Ambrose, J.C., Shoji, T., Kotzer, A.M., Pighin, J.A., and Wasteneys, G.O. (2007). The Arabidopsis CLASP gene encodes a microtubule-associated protein involved in cell expansion and division. Plant Cell *19*, 2763–2775.

Ambrose, C., Allard, J.F., Cytrynbaum, E.N., and Wasteneys, G.O. (2011). A CLASP-modulated cell edge barrier mechanism drives cell-wide cortical microtubule organization in Arabidopsis. Nat. Commun. *2*, 430.

Baena-López, L.A., Baonza, A., and García-Bellido, A. (2005). The orientation of cell divisions determines the shape of Drosophila organs. Curr. Biol. *15*, 1640–1644.

Bennett, T., van den Toorn, A., Sanchez-Perez, G.F., Campilho, A., Willemsen, V., Snel, B., and Scheres, B. (2010). SOMBRERO, BEARSKIN1, and BEAR-SKIN2 regulate root cap maturation in Arabidopsis. Plant Cell *22*, 640–654.

Blilou, I., Xu, J., Wildwater, M., Willemsen, V., Paponov, I., Friml, J., Heidstra, R., Aida, M., Palme, K., and Scheres, B. (2005). The PIN auxin efflux facilitator network controls growth and patterning in Arabidopsis roots. Nature *433*, 39–44.

Brady, S.M., Orlando, D.A., Lee, J.Y., Wang, J.Y., Koch, J., Dinneny, J.R., Mace, D., Ohler, U., and Benfey, P.N. (2007). A high-resolution root spatiotemporal map reveals dominant expression patterns. Science *318*, 801–806.

Camilleri, C., Azimzadeh, J., Pastuglia, M., Bellini, C., Grandjean, O., and Bouchez, D. (2002). The Arabidopsis TONNEAU2 gene encodes a putative novel protein phosphatase 2A regulatory subunit essential for the control of the cortical cytoskeleton. Plant Cell *14*, 833–845.

Campilho, A., Garcia, B., Toorn, H.V., Wijk, H.V., Campilho, A., and S... (2006). Time-lapse analysis of stem-cell divisions in the Arabidopsis thaliana root meristem. Plant J. *48*, 619–627.

Chan, J., Jensen, C.G., Jensen, L.C., Bush, M., a... C.W. (... The 65-kDa carrot microtubule-associated protei... ms re... rly arra... filamentous cross-bridges between microtub... Proc. N... Acad. S... USA *96*, 14931–14936.

De Smet, I., and Beeckman, T. (201... symme... ll division in land plants and algae: the driving force fo... erentiation. N... v. Mol. Cell Biol. *12*, 177–188.

De Smet, I., Vassileva, V., De Ry... l, B., Le... ue, M.P., Grunewald, W., Van Damme, D., Van Noorden... Naudts, M., V... terdael, G., De Clercq, R., et al. (2008). Recepto... kinase ACR4 restric... mative cell divisions in the Arabidopsis root... ence *32... 94–597.

De Smet, I., Lau, S., ... U... neste, S. Benjamins, R., Rademacher, E.H., Schlereth, A., De Ryb... ssileva, V... unewald, W., et al. (2010). Bimod-ular auxin... e contr... rgano... sis in Arabidopsis. Proc. Natl. Acad. Sci. US... 7, 2... 2710.

Dh... siri, N., D... masiri, S., and Estelle, M. (2005a). The F-box protein TIR1 is an... re... 5, 441–445.

Dharmas... Dharmasiri, S., Weijers, D., Lechner, E., Yamada, M., Hobbie, L., Ehrismar... ., Jürgens, G., and Estelle, M. (2005b). Plant development is regulated by a... y of auxin receptor F box proteins. Dev. Cell *9*, 109–119.

Dhonukshe, P., Mathur, J., Hülskamp, M., and Gadella, T.W., Jr. (2005). Microtubule plus-ends reveal essential links between intracellular polarization and localized modulation of endocytosis during division-plane establishment in plant cells. BMC Biol. *3*, 11.

Dhonukshe, P., Baluska, F., Schlicht, M., Hlavacka, A., Samaj, J., Friml, J., and Gadella, T.W., Jr. (2006). Endocytosis of cell surface material mediates cell plate formation during plant cytokinesis. Dev. Cell *10*, 137–150.

Dhonukshe, P., Tanaka, H., Goh, T., Ebine, K., Mähönen, A.P., Prasad, K., Blilou, I., Geldner, N., Xu, J., Uemura, T., et al. (2008). Generation of cell polarity in plants links endocytosis, auxin distribution and cell fate decisions. Nature *456*, 962–966.

Di Laurenzio, L., Wysocka-Diller, J., Malamy, J.E., Pysh, L., Helariutta, Y., Freshour, G., Hahn, M.G., Feldmann, K.A., and Benfey, P.N. (1996). The SCARECROW gene regulates an asymmetric cell division that is essential for generating the radial organization of the Arabidopsis root. Cell *86*, 423–433.

Dolan, L., Janmaat, K., Willemsen, V., Linstead, P., Poethig, S., Roberts, K., and Scheres, B. (1993). Cellular organisation of the Arabidopsis thaliana root. Development *119*, 71–84.

Eren, E.C., Dixit, R., and Gautam, N. (2010). A three-dimensional computer simulation model reveals the mechanisms for self... ation of plant cortical microtubules into oblique arrays. Mol. Biol. C... 7, 20... 84.

Fache, V., Gaillard, J., Van Damme, D... len, D., Neu... E., Stoppin-Mellet, V., and Vantard, M. (2010). Arabid... kinetochore... er-associated MAP65-4 cross-links microtubules... d promo... microtubu... ndle elonga-tion. Plant Cell *22*, 3804–3815.

Gaillard, J., Neumann, E... Damm... ., Stop... ellet, V., Ebel, C., Barbier, E., Geelen, D., an... ntard... 2008). Two microtubule-associated proteins of Arabidop... MAP... ote anti... el microtubule bundling. Mol. Biol. Cell *19*... 4544.

Galinha, C., H... H., Luijten, M... en, V., Blilou, I., Heidstra, R., and Scheres, B... 7). P... THORA proteins... dose-dependent master regulators of Arabidops... root de... ment. Nature *449*, 1053–1057.

Gran... ., and Cyr, ... 2001). Spatiotemporal relationships between g... and microtubule orien... on as revealed in living root cells of Arabidop-... thaliana transformed with green-fluorescent-protein gene construct ... P-MBD. Proto... ma *216*, 201–214.

G... eisen, V.A... J., Marée, A.F., Hogeweg, P., and Scheres, B. (2007). Au... nsport... sufficient to generate a maximum and gradient guiding root g... ure *449*, 1008–1013.

... ilfoyle, T.J., and Hagen, G. (2007). Auxin response factors. Curr. Opin. Plant ... 453–460.

Gunning, B., Hughes, J., and Hardham, A. (1978). Formative and Proliferative Cell Divisions, Cell Differentiation, and Developmental Changes in the Meri-stem of Azolla Roots. Planta *143*, 121–144.

Hamann, T., Mayer, U., and Jürgens, G. (1999). The auxin-insensitive bodenlos mutation affects primary root formation and apical-basal patterning in the Arabidopsis embryo. Development *126*, 1387–1395.

Hardtke, C.S., and Berleth, T. (1998). The Arabidopsis gene MONOPTEROS encodes a transcription factor mediating embryo axis formation and vascular development. EMBO J. *17*, 1405–1411.

Hayashi, K., Tan, X., Zheng, N., Hatate, T., Kimura, Y., Kepinski, S., and Nozaki, H. (2008). Small-molecule agonists and antagonists of F-box protein-substrate interactions in auxin perception and signaling. Proc. Natl. Acad. Sci. USA *105*, 5632–5637.

Heidstra, R., Welch, D., and Scheres, B. (2004). Mosaic analyses using marked activation and deletion clones dissect Arabidopsis SCARECROW action in asymmetric cell division. Genes Dev. *18*, 1964–1969.

Heisler, M.G., Ohno, C., Das, P., Sieber, P., Reddy, G.V., Long, J.A., and Meyerowitz, E.M. (2005). Patterns of auxin transport and gene expression during primordium development revealed by live imaging of the Arabidopsis inflorescence meristem. Curr. Biol. *15*, 1899–1911.

Helariutta, Y., Fukaki, H., Wysocka-Diller, J., Nakajima, K., Jung, J., Sena, G., Hauser, M.T., and Benfey, P.N. (2000). The SHORT-ROOT gene controls radial patterning of the Arabidopsis root through radial signaling. Cell *101*, 555–567.

Jürgens, G. (1995). Axis formation in plant embryogenesis: cues and clues. Cell *81*, 467–470.

Kares, C., Prinsen, E., van Onckelen, H., and Otten, L. (1990). IAA synthesis and root induction with iaa genes under heat shock promoter control. Plant. Mol. Biol. *15*, 225–236.

Kepinski, S., and Leyser, O. (2005). The Arabidopsis F-box protein TIR1 is an auxin receptor. Nature *435*, 446–451.

Kirik, V., Herrmann, U., Parupalli, C., Sedbrook, J.C., Ehrhardt, D.W., and Hülskamp, M. (2007). CLASP localizes in two discrete patterns on cortical microtubules and is required for cell morphogenesis and cell division in Arabidopsis. J. Cell Sci. *120*, 4416–4425.

Lau, S., De Smet, I., Kolb, M., Meinhardt, H., and Jürgens, G. (2011). Auxin trig-gers a genetic switch. Nat. Cell Biol. *13*, 611–615.

Li, H., Zeng, X., Liu, Z.Q., Meng, Q.T., Yuan, M., and Mao, T.L. (2009). Arabidopsis microtubule-associated protein AtMAP65-2 acts as a microtubule stabilizer. Plant Mol. Biol. *69*, 313–324.

Lucas, J.R., Courtney, S., Hassfurder, M., Dhingra, S., Bryant, A., and Shaw, S.L. (2011). Microtubule-associated proteins MAP65-1 and MAP65-2 positively regulate axial cell growth in etiolated Arabidopsis hypocotyls. Plant Cell *23*, 1889–1903.

Manders, E.M., Stap, J., Brakenhoff, G.J., van Driel, R., and Aten, J.A. (1992). Dynamics of three-dimensional replication patterns during the S-phase, analysed by double labelling of DNA and confocal microscopy. J. Cell Sci. *103*, 857–862.

Müller, S., Wright, A.J., and Smith, L.G. (2009). Division plane control in plants: new players in the band. Trends Cell Biol. *19*, 180–188.

Nakajima, K., Sena, G., Nawy, T., and Benfey, P.N. (2001). Intercellular movement of the putative transcription factor SHR in root patterning. Nature *413*, 307–311.

Péret, B., De Rybel, B., Casimiro, I., Benková, E., Swarup, R., Laplaze, L., Beeckman, T., and Bennett, M.J. (2009). Arabidopsis lateral root development: an emerging story. Trends Plant Sci. *14*, 399–408.

Petersson, S.V., Johansson, A.I., Kowalczyk, M., Makoveychuk, A., Wang, J.Y., Moritz, T., Grebe, M., Benfey, P.N., Sandberg, G., and Ljung, K. (2009). An auxin gradient and maximum in the Arabidopsis root apex shown by high-resolution cell-specific analysis of IAA distribution and synthesis. Plant Cell *21*, 1659–1668.

Petricka, J.J., Van Norman, J.M., and Benfey, P.N. (2009). Symmetry breaking in plants: molecular mechanisms regulating asymmetric cell divisions in Arabidopsis. Cold Spring Harb Perspect Biol *1*, a000497.

Pickett-Heaps, J.D., and Northcote, D.H. (1966). Organization of microtubules and endoplasmic reticulum during mitosis and cytokinesis in wheat meristems. J. Cell Sci. *1*, 109–120.

Rasmussen, C.G., Humphries, J.A., and Smith, L.G. (2011a). Determination of symmetric and asymmetric division planes in plant cells. Annu. Rev. Plant Biol. *62*, 387–409.

Rasmussen, C.G., Sun, B., and Smith, L.G. (2011b). Tangled localization at the cortical division site of plant cells occurs by several mechanisms. J. Cell Sci. *124*, 270–279.

Sabatini, S., Beis, D., Wolkenfelt, H., Murfett, J., Guilfoyle, T., Malamy, J., Benfey, P., Leyser, O., Bechtold, N., Weisbeek, P., and Scheres, B. (1999). An auxin-dependent distal organizer of pattern and polarity in the Arabidopsis root. Cell *99*, 463–472.

Smertenko, A., Saleh, N., Igarashi, H., Mori, H., Hauser-Hahn, I., Jiang, C.J., Sonobe, S., Lloyd, C.W., and Hussey, P.J. (2000). A new class of microtubule-associated proteins in plants. Nat. Cell Biol. *2*, 750–753.

Smertenko, A.P., Kaloriti, D., Chang, H.Y., Fiserova, J., Opatrny, Z., and Hussey, P.J. (2008). The C-terminal variable region specifies the dynamic properties of Arabidopsis microtubule-associated protein MAP65 isotypes. Plant Cell *20*, 3346–3358.

Smith, L.G. (2001). Plant cell division: building walls in the right places. Nat. Rev. Mol. Cell Biol. *2*, 33–39.

Staswick, P.E., Serban, B., Rowe, M., Tiryaki, I., Maldonado, M.T., Maldonado, M.C., and Suza, W. (2005). Characterization of an Arabidopsis enzyme family that conjugates amino acids to indole-3-acetic acid. Plant Cell *17*, 616–627.

ten Hove, C.A., Willemsen, V., de Vries, W.J., van Dijken, A., Scheres, B., and Heidstra, R. (2010). SCHIZORIZA encodes a nuclear factor regulating asymmetry of stem cell divisions in the Arabidopsis root. Curr. Biol. *20*, 452–457.

Tindemans, S.H., Hawkins, R.J., and Mulder, B.M. (2010). Survival of the aligned: ordering of the plant cortical microtubule array. Phys. Rev. Lett. *104*, 058103.

Torres-Ruiz, R.A., and Jürgens, G. (1994). Mutations in the FASS gene uncouple pattern formation and morphogenesis in Arabidopsis development. Development *120*, 2967–2978.

Traas, J., Bellini, C., Nacry, P., Kronenberger, J., Bouchez, D., and Caboche, M. (1995). Normal differentiation patterns in plants lacking microtubular preprophase bands. Nature *375*, 676–677.

Tromas, A., Braun, N., Muller, P., Khodus, T., Paponov, I.A., Palme, K., Ljung, K., Lee, J.Y., Benfey, P., Murray, J.A., et al. (2009). The AUXIN BINDING PROTEIN 1 is required for differential auxin responses mediating root growth. PLoS ONE *4*, e6648.

Ueda, K., Matsuyama, T., and Hashimoto, T. (1999). Visualization of microtubules in living cells of transgenic Arabidopsis thaliana. Protoplasma *206*, 201–206.

Van Damme, D., Van Poucke, K., Boutant, E., Ritzenthaler, C., Inzé, D., and Geelen, D. (2004). In vivo dynamics and differential microtubule-binding activities of MAP65 proteins. Plant Physiol. *136*, 3956–3967.

Wasteneys, G.O., and Ambrose, J.C. (2009). Spatial organization of plant cortical microtubules: close encounters of the 2D kind. Trends Cell Biol. *19*, 62–71.

Willemsen, V., Bauch, M., Bennett, T., Campilho, A., Wolkenfelt, H., Xu, J., Haseloff, J., and Scheres, B. (2008). The NAC domain transcription factors FEZ and SOMBRERO control the orientation of cell division plane in Arabidopsis root stem cells. Dev. Cell *15*, 913–922.

Xu, J., Hofhuis, H., Heidstra, R., Sauer, M., Friml, J., and Scheres, B. (2006). A molecular framework for plant regeneration. Science *311*, 385–388.